

Constraints on ultra-slow-roll inflation with the NANOGrav 15-Year Dataset

Bo Mu,^{a,b} Jing Liu,^{a,b} Gong Cheng,^{a,b} Zong-Kuan Guo,^{c,d,e}

^aInternational Centre for Theoretical Physics Asia-Pacific, University of Chinese Academy of Sciences, 100190 Beijing, China

^bTaiji Laboratory for Gravitational Wave Universe, University of Chinese Academy of Sciences, 100049 Beijing, China

^cCAS Key Laboratory of Theoretical Physics, Institute of Theoretical Physics, Chinese Academy of Sciences, P.O. Box 2735, Beijing 100190, China

^dSchool of Physical Sciences, University of Chinese Academy of Sciences, No.19A Yuquan Road, Beijing 100049, China

^eSchool of Fundamental Physics and Mathematical Sciences, Hangzhou Institute for Advanced Study, University of Chinese Academy of Sciences, Hangzhou 310024, China

E-mail: mubo22@mailsucas.ac.cn, liujing@ucas.ac.cn, chenggong@ucas.ac.cn, guozk@itp.ac.cn

Abstract. Ultra-slow-roll (USR) inflation predicts an exponential amplification of scalar perturbations at small scales, which leads to a stochastic gravitational wave background (SGWB) through the coupling of the scalar and tensor modes at the second-order expansion of the Einstein equation. In this work, we search for such a scalar-induced SGWB from the NANOGrav 15-year (NG15) dataset, and find that the SGWB from USR inflation could explain the observed data. The Bayes factors are 54 ± 5 for the USR inflation model alone and 68 ± 6 for the combined USR inflation plus supermassive black hole binaries (SMBHB) models. We place constraints on the amplitude of the scalar power spectrum to $P_{\text{Rp}} > 10^{-1.95}$ at 95% confidence level (C.L.) at the scale of $k \sim 20 \text{ pc}^{-1}$. We find that $\log_{10} P_{\text{Rp}}$ degenerates with the peak scale $\log_{10} k_{\text{p}}$. We also obtain the parameter space allowed by the data in the USR inflationary scenario, where the e -folding numbers of the duration of the USR phase has a lower limit $\Delta N > 2.80$ (95% C.L.) when the USR phase ends at $N \approx 20$. With astrophysically motivated priors, the NG15 dataset fits both the USR inflation model and SMBHB model equally well.

Contents

1	Introduction	1
2	PTA Data	2
3	SGWB from USR inflation	3
4	Results	5
5	Conclusions and discussions	9
A	The choice of γ value	12

1 Introduction

The direct detection of gravitational waves (GWs), which are the ripples of spacetime predicted by general relativity, opens a new era of the exploration of the early Universe [1–3]. The monumental discovery was the detection of the merger of two black holes by LIGO which provides a new way to observe the Universe, complementing traditional electromagnetic observations. SGWBs are formed from the superpositions of many unresolved GW sources, of both astrophysical and cosmological origins, which can be detected by searching for correlated signals between multiple detectors. Searching for such SGWBs has been the main scientific goal of multiband GW observers including LIGO-Virgo-KAGRA, LISA, Taiji, TianQin, and pulsar timing array (PTA) experiments.

Recently, the PTA experiments, including CPTA [4], NANOGrav [5], PPTA [6] and EPTA [7], collectively announced the first positive evidence of SGWBs at the nanohertz frequency band ($\sim 1 - 100$ nHz). Based on the evolution of the Universe, it is predicted that a cosmic population of supermassive black hole binaries generates an SGWB at the nanohertz frequency band, which is treated as the fiducial model in the analysis of NANOGrav-15 dataset [8]. However, the detected GW power spectrum deviates from that given by the expected values of each parameter [9]. Actually there are also other potential GW sources at this frequency band, such as cosmological phase transitions [10–12], cosmic topological defects [13–17], and primordial scalar perturbations [18–34], which generate SGWBs in the early Universe. It is found that some of these cosmological sources can explain the NANOGrav dataset [5]. In their work, three parameterization templates for the power spectrum of scalar perturbations, which source the energy spectrum of scalar-induced gravitational waves (SIGWs), have been considered.

In this paper, we fit the NG15 dataset with the SGWB from ultra-slow-roll (USR) inflation (marked as SIGW-USR in this paper), which is a physically well-motivated SIGW model. In the USR inflationary scenario, where the slow-roll approximation is not adhered to, the superhorizon evolution of scalar perturbations can lead to exponential amplification as calculated in various studies [35–37]. The USR regime arises from the non-attractor evolution of the inflaton field, which can be manifested through modified gravity theories [38–42], string theory approaches [43–45], and supergravity models [46–49]. Additionally, minor fluctuations in the inflationary potential – encompassing features like bumps [50, 51], dips [50,

52], inflection points [53–55, 55], and steps [56–59] – might also be considered as possible triggers for the USR regime. A myriad of references [60–75] suggest that enhanced curvature perturbations might pave the way for the emergence of primordial black holes housing dark matter, rendering USR inflation a subject of keen interest. Based on cosmic microwave background (CMB) observations, the amplitude of the primordial scalar power spectrum is firmly constrained to be around 2.10×10^{-9} [76]. Nonetheless, at smaller scales, these constraints might be more flexible [77–79]. The USR domain can also yield significant e -folding numbers, crucial parameters for addressing horizon, flatness, and monopole issues [80]. The core objective of our research is to discern the constraints that the NG15 dataset might impose on the inflationary potential of the USR regime as well as on the power spectrum of scalar perturbations. For convenience, $c = 8\pi G = 1$ is set throughout this paper.

2 PTA Data

We use the NG15 dataset, which comprises the pulse time of arrival (ToAs) for 68 millisecond pulsars. With a timing baseline of 3 years, 67 of these pulsars remain viable for processing. NANOGrav fits these ToAs to a timing model that encapsulates the sky location, proper motion, parallax, pulsar spin period, and spin period derivative for each pulsar [8].

We use the Python package `PTArcade` [81] to perform the Bayesian analysis, which integrates new physics into the PTA data analysis package `ENTERPRISE` [82]. New physics is characterized by the GW spectrum, denoted as Ω_{GW} . Except for Ω_{GW} , we set other parameters by default, such as the ephemeris model included in the timing model.

Then, we will briefly introduce the likelihood function used in this work. The pulsar’s timing residuals δt can be modeled as

$$\delta t = \mathbf{n} + \mathbf{M}\boldsymbol{\epsilon} + \mathbf{F}\mathbf{a}, \quad (2.1)$$

where \mathbf{n} describes the white noise, $\mathbf{M}\boldsymbol{\epsilon}$ represents the errors associated with the best-fitting timing-ephemeris parameters [83]. The term $\mathbf{F}\mathbf{a}$ characterizes the red noise, which is presumed to be a combination of pulsar-intrinsic red noise and SGWB signals. The matrix \mathbf{F} is the Fourier basis matrix, constructed from sine-cosine pairs based on the ToAs with frequencies defined as $f_i = i/T_{\text{obs}}$, where $T_{\text{obs}} = 16.03\text{yr}$ is the timing baseline for the entire NG15 dataset. For the Fourier amplitudes, \mathbf{a} follows a zero-mean normal distribution with a covariance matrix $\langle \mathbf{a}\mathbf{a}^T \rangle = \boldsymbol{\phi}$, which is given by

$$[\phi]_{(ak)(bj)} = \delta_{ij} (\delta_{ab}\varphi_{a,i} + \Gamma_{ab}\Phi_i). \quad (2.2)$$

The first term characterizes the pulsar-intrinsic red noise, which is defined as a power-law function in this work, with the coefficients $\varphi_{a,i}$ modeled as

$$\varphi_{a,i}(f) = \frac{A_a^2}{12\pi^2 T_{\text{obs}}} \left(\frac{f}{1\text{yr}^{-1}} \right)^{-\gamma_a} \text{yr}^3, \quad (2.3)$$

and the priors of A_a, γ_a are shown in Table I. In the second term, Γ_{ab} is defined based on the Hellings & Downs (“HD”) correlation [84]. Φ_i is related to the SGWB spectrum as

$$\Omega_{\text{GW}}(f) \equiv \frac{1}{\rho_c} \frac{d\rho_{\text{GW}}(f)}{d\ln(f)} = \frac{8\pi^4 f^5}{H_0^2} \frac{\Phi(f)}{\Delta f}. \quad (2.4)$$

Here $H_0 = h \times 100 \text{ km s}^{-1} \text{Mpc}^{-1}$ is the Hubble constant, $\Delta f = 1/T_{\text{obs}}$, and $\Phi(f)$ is defined as $\Phi_i = \Phi(i/T_{\text{obs}})$.

Upon marginalizing over \mathbf{a}, ϵ , we obtain a likelihood that depends only on the parameters that affect $\langle \mathbf{a}\mathbf{a}^T \rangle$. The likelihood is expressed as

$$p(\delta\mathbf{t}|\phi) = \frac{\exp\left(-\frac{1}{2}\delta\mathbf{t}^T \mathbf{C}^{-1} \delta\mathbf{t}\right)}{\sqrt{\det(2\pi\mathbf{C})}}, \quad (2.5)$$

where $\mathbf{C} = \mathbf{N} + \mathbf{T}\mathbf{B}\mathbf{T}^T$, \mathbf{N} is the covariance matrix of \mathbf{n} , $\mathbf{T} = [\mathbf{M}, \mathbf{F}]$, and $\mathbf{B} = \text{diag}(\infty, \phi)$. Here, ∞ represents a diagonal matrix filled with infinities, implying that the priors for parameters in ϵ are assumed to be flat.

3 SGWB from USR inflation

Under the slow-roll approximation, the Fourier modes of curvature perturbations, R_k , remain constant at superhorizon scales. Refs. [35–37] find that during the USR regime at superhorizon scales, the time derivative of R_k , denoted as \dot{R}_k , undergoes exponential amplification. Consequently, the primordial scalar power spectrum P_R derived from R_k reaches its peak at the beginning of USR inflation. Ref. [35] suggests that P_R behaves as $P_R \propto k^4$ on the infrared side of the peak, and $P_R \propto k^\beta$ on the ultraviolet side, with β depending on the inflationary potential. Given that USR inflation ends at $\phi = \phi_e$, the Taylor expansion of the inflationary potential around ϕ_e is

$$V(\phi) = b_0 + b_1(\phi - \phi_e) + b_2(\phi - \phi_e)^2 + \dots \quad (3.1)$$

In a Friedmann-Robertson-Walker universe, the Friedmann equation and the EOM of ϕ are written as

$$\begin{aligned} H^2 &= \frac{1}{3} \left(\dot{\phi}^2 + V(\phi) \right), \\ \ddot{\phi} + 3H\dot{\phi} + \frac{dV}{d\phi} &= 0, \end{aligned} \quad (3.2)$$

and with $|\dot{\phi}|$ reaches its minimum at t_e , we can obtain

$$\begin{aligned} \ddot{\phi}(t_e) &= 0, \\ 3H\dot{\phi}(t_e) &= -\frac{dV}{d\phi}(t_e) = -b_1, \end{aligned} \quad (3.3)$$

With more detailed assumptions and further calculation [35], one can obtain

$$\beta = 3 - \sqrt{9 - 24b_2/b_0}, \quad (3.4)$$

which can be treated as a constant as long as ϕ is in the vicinity of ϕ_e . During the USR regime $\dot{\phi}$ exponentially decreases, after which ϕ stays close to ϕ_e for a long period during inflation so that the expansion (3.1) remains valid. Due to the smallness of $\dot{\phi}(t_e)$, the parameter b_1 should also be very small. Note that the spectral index of the amplified $P_R(k)$ is independent of the linear term in Eq. (3.1). The term $\dot{\phi}$ exponentially decreases in the short USR regime, reaching its minimum at t_e . Subsequently, $\dot{\phi}$ needs to increase significantly to ensure a successful end of inflation. Apart from the rather short period around t_e , the term $\dot{\phi}$ is orders

of magnitude larger than its minimum value, leading to the dominance of the dynamics of ϕ and the profile of $P_R(k)$ by the quadratic term, $b_2(\phi - \phi_e)^2$, in $V(\phi)$.

Instead of numerically calculating the exact form of $P_R(k)$, we parameterize the power spectrum of curvature perturbations in USR inflation as

$$P_R(k) = P_{Rp} \frac{(\alpha + \beta)^\gamma}{\left[\beta (k/k_p)^{-\alpha/\gamma} + \alpha (k/k_p)^{\beta/\gamma} \right]^\gamma}, \quad (3.5)$$

where $P_R(k)$ reaches its peak value P_{Rp} at $k = k_p$, and we set $\alpha = 4$ following the relation $P_R \propto k^4$. The parameter γ characterizes the smoothness of $P_R(k)$ around the peak. Since γ does not significantly affect the results, we adopt a representative value of $\gamma = 2.6$ in this work. The justification for this selection is detailed in the appendix. Then, the remaining free parameters are P_{Rp} , k_p , and β .

Given the form of $P_R(k)$, we are able to numerically calculate the GW energy spectrum $\bar{\Omega}_{\text{GW}}(k)$ in the radiation-dominated era, following the integration method in Refs. [85, 86]

$$\bar{\Omega}_{\text{GW}}(k) = \int_0^\infty dv \int_{|1-v|}^{1+v} du \left(\frac{4v^2 - (1 + v^2 - u^2)^2}{4uv} \right)^2 \text{IRD}_{sq}(u, v) P_R(ku) P_R(kv), \quad (3.6)$$

in which $\text{IRD}_{sq}(u, v)$ is a function of u, v ,

$$\begin{aligned} \text{IRD}_{sq}(u, v) = & \frac{1}{2} \left(\frac{3(u^2 + v^2 - 3)^2}{4u^3v^3} \right)^2 \times \left[\left(-4uv + (u^2 + v^2 - 3) \ln \left| \frac{3 - (u+v)^2}{3 - (u-v)^2} \right| \right)^2 \right. \\ & \left. + \pi^2 (u^2 + v^2 - 3)^2 \Theta(u + v - \sqrt{3}) \right], \end{aligned} \quad (3.7)$$

where $\Theta(x)$ is the heaviside step function.

Furthermore, using the relationship $f \approx 0.03 \text{ Hz} \frac{k}{2 \times 10^7 \text{ pc}^{-1}}$, we could express $\bar{\Omega}_{\text{GW}}(k)$ in terms of the corresponding frequency f . Repeatedly calculating this integration for every step would be computationally expensive. As the integral is simply proportional to P_{Rp}^2 , we extract P_{Rp}^2 from the integral. So now the integral only depends on the other two parameters β and f_p . Then we compute the integration in the β - f_p grid. So for any given values of β and f_p , we can infer the integral by using 2-D interpolation.

The energy spectrum of SGWB at present $\Omega_{\text{GW}}(f)$ is related to $\bar{\Omega}_{\text{GW}}(f)$ as

$$\Omega_{\text{GW}}(f) = \Omega_r \left(\frac{g_*(f)}{g_*^0} \right) \left(\frac{g_{*,s}^0}{g_{*,s}(f)} \right)^{4/3} \bar{\Omega}_{\text{GW}}(f), \quad (3.8)$$

where Ω_r is the present energy density fraction of radiation, g_* and $g_{*,s}$ respectively represent the effective relativistic degree of freedom that contribute to the radiation energy and entropy density, the superscript 0 denotes the present time. To determine $\Omega_{\text{GW}}(f)$, we set the values $\Omega_r/g_*^0 \approx 2.72 \times 10^{-5}$, $g_{*,s}^0 \approx 3.93$, and the functions $g_*(f)$ and $g_{*,s}(f)$ given in Ref. [87].

The priors adopted in this work are listed in Table I. By definition, the peak value P_{Rp} should not exceed $\mathcal{O}(1)$ so that R_k remains at the level of perturbations. Thus we set $\log_{10} P_{Rp} \leq 0$ to explore what constraints the NG15 dataset would impose on the USR model. Curvature perturbations with large amplitude are also responsible to the production of primordial black holes (PBHs). To avoid the overproduction of PBHs, we also apply a

Table 1. Priors on the Model Parameters. The first five parameters correspond to our USR model, while the 2-D Gaussian prior is applied to the SMBHB model. The exact values for μ_{BHB} and σ_{BHB} are introduced in Eq.(3.9). For P_{Rp} , we impose an upper limit of $\log_{10}P_{Rp} \leq 0$, disregarding astrophysical constraints, to explore what constraints the NG-15 dataset would impose on the USR model. Additionally, a more stringent upper limit of $\log_{10}P_{Rp} \leq -2$ is set based on PBH abundance, allowing for comparison with the SMBHB model under astrophysically motivated priors.

Parameters	Priors
P_{Rp}	Log-Uniform($-3, -2/0$)
f_p [Hz]	Log-Uniform($-10, -5$)
α	4
β	Uniform($0, 5$)
γ	2.6
$(\log_{10}A_{\text{BHB}}, \gamma_{\text{BHB}})$	Normal($\mu_{\text{BHB}}, \sigma_{\text{BHB}}$)

conservative upper bound $\log_{10}P_{Rp} \leq -2$ for Gaussian perturbations. [31] There is no prior information for f_p since the USR regime can occur at any period during inflation. Therefore, we set f_p to be roughly within the sensitivity band of NANOGrav. The energy spectrum in our model is a convex upward curve. If f_p is below the band of NANOGrav, the spectrum can not fit the data. But if f_p is beyond the band of NANOGrav, our model can still fit the data well. So we set the upper bound of the prior for f_p two orders of magnitude higher than the band of NANOGrav. For the parameter β , theoretically it can span a large range, so we set the prior of β between 0 and 5 to study its behavior. As the GWB from the mergers of SMBHBs is a promising signal in the PTA band, we explore the possibility of using a combined signal model that incorporates both SIGW-USR model and SMBHB model (SIGW-USR+SMBHB) to explain the NANOGrav dataset. The spectrum of SMBHB takes the form similar to Eq.(2.4), with $\Phi(f)$ similar to Eq.(2.3). The priors of SMBHB are set by the Python package `PTArcade` by default (see the appendix of Ref. [5] for details). We list the parameter values for the 2-D Gaussian prior of the SMBHB model below.

$$\mu_{\text{BHB}} = \begin{pmatrix} -15.6 \\ 4.7 \end{pmatrix}, \sigma_{\text{BHB}} = \begin{pmatrix} 2.8 & -0.026 \\ -0.026 & 1.2 \end{pmatrix} \quad (3.9)$$

4 Results

We use the SGWB energy spectrum from SIGW-USR and the combined model SIGW-USR+SMBHB to fit the NG15 dataset and obtain the constraints on the model parameters. Fig. 1 shows the posterior distributions for the three model parameters. We also calculate the Bayes factors against the baseline SMBHB model, yielding $\mathcal{B} = 54 \pm 5$ for SIGW-USR and $\mathcal{B} = 68 \pm 6$ for SIGW-USR+SMBHB. To compare with the Bayes factors obtained by other new physics models, we use the same prior for P_{Rp} when calculating these two Bayes factors as in the SIGW models mentioned in Ref. [5], which follows a log-uniform distribution $(-3, 1)$. The Bayes factors are close to those for the SIGW-Gauss model, the best-fitting model for the NG15 dataset reported in Ref. [5]. This suggests the SIGW-USR model also provides a good fit for the NG15 dataset.

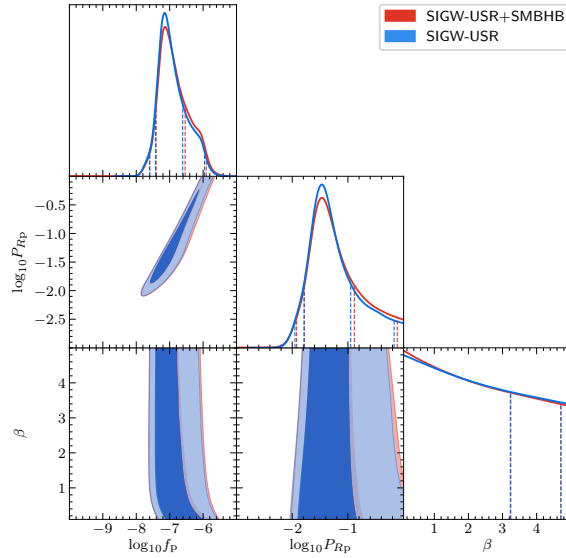


Figure 1. Posterior distribution of three input parameters. The red and blue contours denote the 68% and 95% confidence regions of SIGW-USR and SIGW-USR+SMBHB, respectively.

As the PTA data points are roughly monotonically increasing, in the posterior plot, the peak of Ω_{GW} will degenerate with f_p . And the peak of $\log_{10} \Omega_{\text{GW}}$ is proportional to $\log_{10} P_{\text{Rp}}$, so we find that in the $\log_{10} P_{\text{Rp}} - \log_{10} f_p$ plot, the two parameters degenerate with each other. The degeneracy could also be found in the power-law energy spectrum model. The lower limit of $\log_{10} P_{\text{Rp}}$ is approximately -1.95 at 95% C.L. for SIGW-USR and SIGW-USR+SMBHB. In the one-dimensional marginalized distribution, the peak values of $\log_{10} P_{\text{Rp}}$ and $\log_{10} f_p$ are -1.46 and -7.14 for SIGW-USR, -1.47 and -7.14 for SIGW-USR+SMBHB, respectively. Besides, the parameter β is poorly constrained as expected.

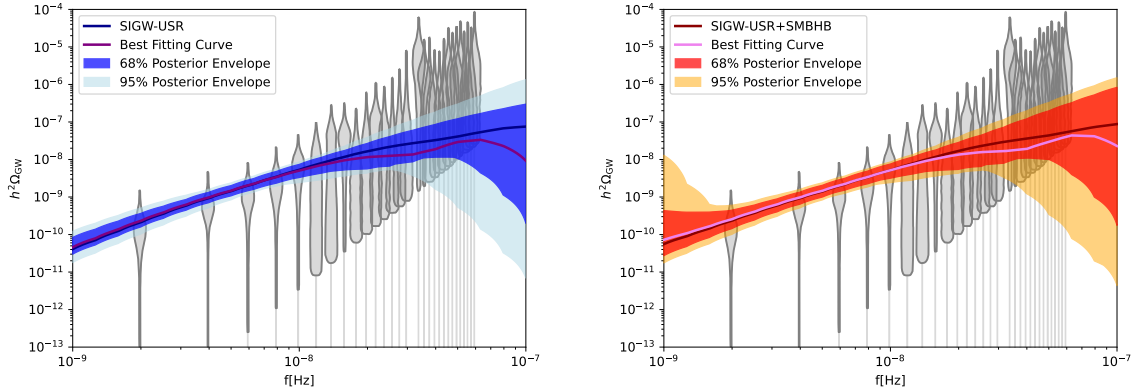


Figure 2. The 68% and 95% posterior envelopes, the best-fitting SGWB power spectra, and the median SGWB power spectra for both the SIGW-USR and SIGW-USR+SMBHB models are shown. The label of the median GW power spectra is used to indicate the corresponding model. The gray violin plots represent the periodogram for the free spectral process from the NANOGrav dataset [5].

In Fig. 2, we present The 68% and 95% posterior envelopes, the best fitting SGWB power spectra and the median GW power spectra of both SIGW-USR and SIGW-USR+SMBHB models, and we plot the NANOGrav data points [5] as well. The energy spectrum in our model is a convex upward curve. So to fit the data, f_p should be at or above the NANOGrav band. The infrared spectrum of our model is governed by the spectrum index α which is a constant in our model. The UV spectrum of our model is governed by the index β . The constraining power of NANOGrav data mostly comes from the low-frequency and intermediate-frequency data points, so β is loosely constrained.

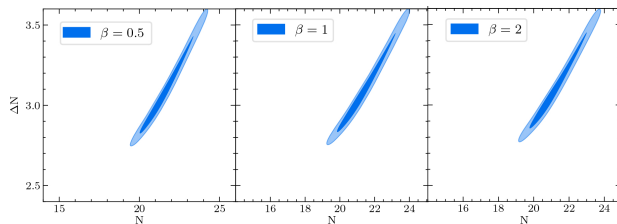


Figure 3. The confidence contours of $N - \Delta N$ with β set as 0.5, 1 and 2 from left to right.

In Fig. 3, we present our constraints on N and ΔN , the intrinsic parameters of USR inflation, where N and ΔN respectively denotes the e -folding number of the end and the duration of the USR regime¹. Through an analytical calculation to predict $P_R(k)$ within the USR inflation framework, we discern the amplification rate of $P_R(k)$ at its peak to be $e^{6\Delta N}$.

The e -folding number of the end of the USR regime can be roughly settled in the range about $N \sim 15 - 50$ since inflation lasts for $60 - 70$ e -foldings. The USR regime may affect the CMB observable if N is too small and the Universe fails to exit inflation if N is too large. Given that $P_R \approx 2 \times 10^{-9}$ at the CMB scales, the range of ΔN should be roughly $0 - 3.3$ to avoid nonlinearities of curvature perturbations. Our fitting results from PTA observations can also be understood as the constraints on ΔN in the range $N \sim 17.5 - 22.5$, shown in Fig. 3. Although the current constraint is relatively loose, the future programs of GW observation, such as SKA, LISA, DECIGO and CE, can provide a much wider and more strict constraint on $P_R(k)$.

The comprehensive consideration of the CMB observable and the PTA results may yield some interesting results. Before the beginning of the USR regime, the rolling of inflaton tends to accelerate due to the steeper potential, rendering a more natural non-attractor phase. The early increase of $\dot{\phi}$ leads to a decrease of P_R in the large scales. If the PTA data originates from the USR inflation, we expect a significant running of the spectral index of curvature perturbations in the more precise measurement of CMB. This explanation can also support double inflation [88] where the inflaton exit the slow-roll regime during inflation and the effective potential has more than one plateau to provide enough e -folds.

To investigate the impact of β on constraints, we chose three typical values 0.5, 1, 2 for β . The posterior distributions indicate that ΔN strongly degenerates with N . As mentioned before, β has little effect on the constraints.

To make a detailed comparison with the SMBHB model, Fig. 4 and Fig. 5 show the posterior distributions and posterior envelopes for the SIGW-USR, SIGW-USR+SMBHB, and SMBHB models, each with their astrophysically motivated priors. For the SIGW-USR

¹ The exact definition of N is $N \equiv \ln[a(t_e)/a(t_i)]$, where a is the scale factor, t_i is the time when the Hubble scale at present leaves the horizon during inflation, and t_e is the end of the USR regime.

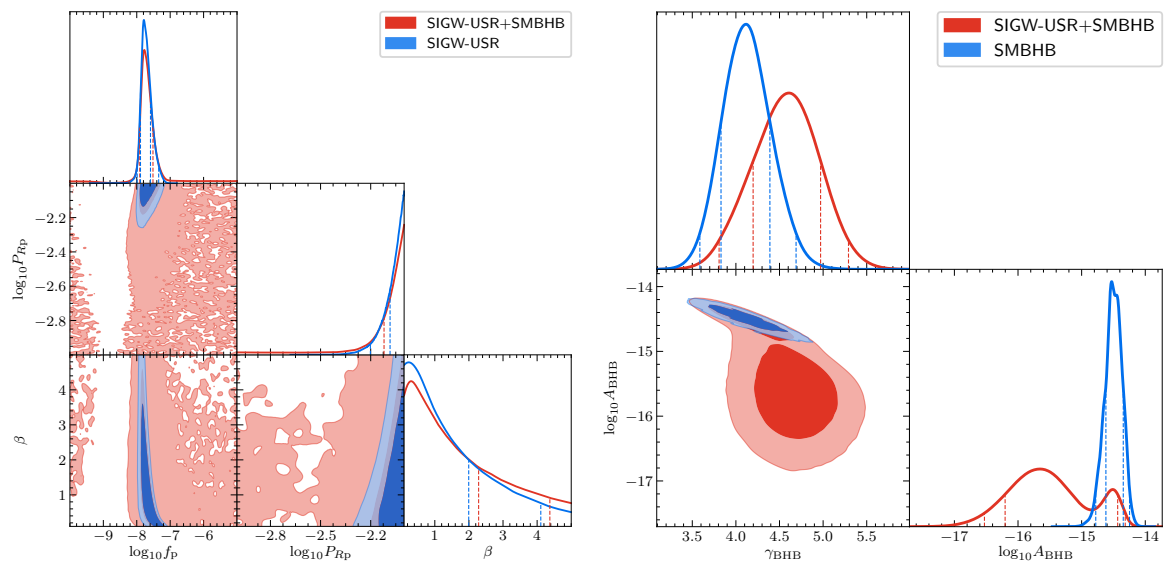


Figure 4. Posterior distribution of three input parameters of SIGW-USR and SIGW-USR+SMBHB with the astrophysically motivated upper limit $\log_{10} P_{Rp} \leq -2$, and of SMBHB model with the 2-D Gaussian prior.

model, the prior is $\log_{10} P_{Rp} \leq -2$, while the SMBHB model uses the 2-D Gaussian prior described in Eq(3.9). The Bayes factors against the SMBHB model are $\mathcal{B} = 3.6 \pm 0.4$ for SIGW-USR and $\mathcal{B} = 6.1 \pm 0.6$ for SIGW-USR+SMBHB, suggesting that, with astrophysically motivated priors, the NG15 dataset fits both the SIGW-USR and SMBHB models similarly well. This is further confirmed by Fig. 5.

In Fig. 4, for the SMBHB model, the 2-D Gaussian prior introduces a smooth cutoff at the upper left end of the confidence contours, leaving some overlap with the 68% confidence contour of Fig. 5 in Ref. [8]. In contrast, for the SIGW-USR model, the upper limit imposes a hard cutoff, thus the blue contours are extensions of the lower left end of the 95% confidence contours in Fig. 1. The confidence contours for the SMBHB parameters in the SIGW-USR+SMBHB model represent a combination of the posterior distributions of the single SMBHB model and the 2-D Gaussian prior. The reasoning for this is introduced in the next paragraph.

In Fig. 5, the 68% and 95% posterior envelopes of the SIGW-USR+SMBHB model can almost be seen as a simple sum of those from the SIGW-USR and SMBHB models. This scenario occurs only when both models fit the NG15 dataset equally well. When models produce curves within their posterior envelopes, they are offering their best likelihoods under the given prior. In the case of SIGW-USR+SMBHB, if one model provides a curve within its own posterior envelope and the other model doesn't significantly detract from the performance, the best likelihood can still be achieved. As seen in the red contours of Fig. 4, in the SMBHB posterior distributions, the upper 68% contour corresponds to the SMBHB model dominating, while the lower 68% contour corresponds to the SIGW-USR model dominating. The red 68% contours also show some expansion, indicating that the combination of these two models enhances the performance of certain insufficient fits.

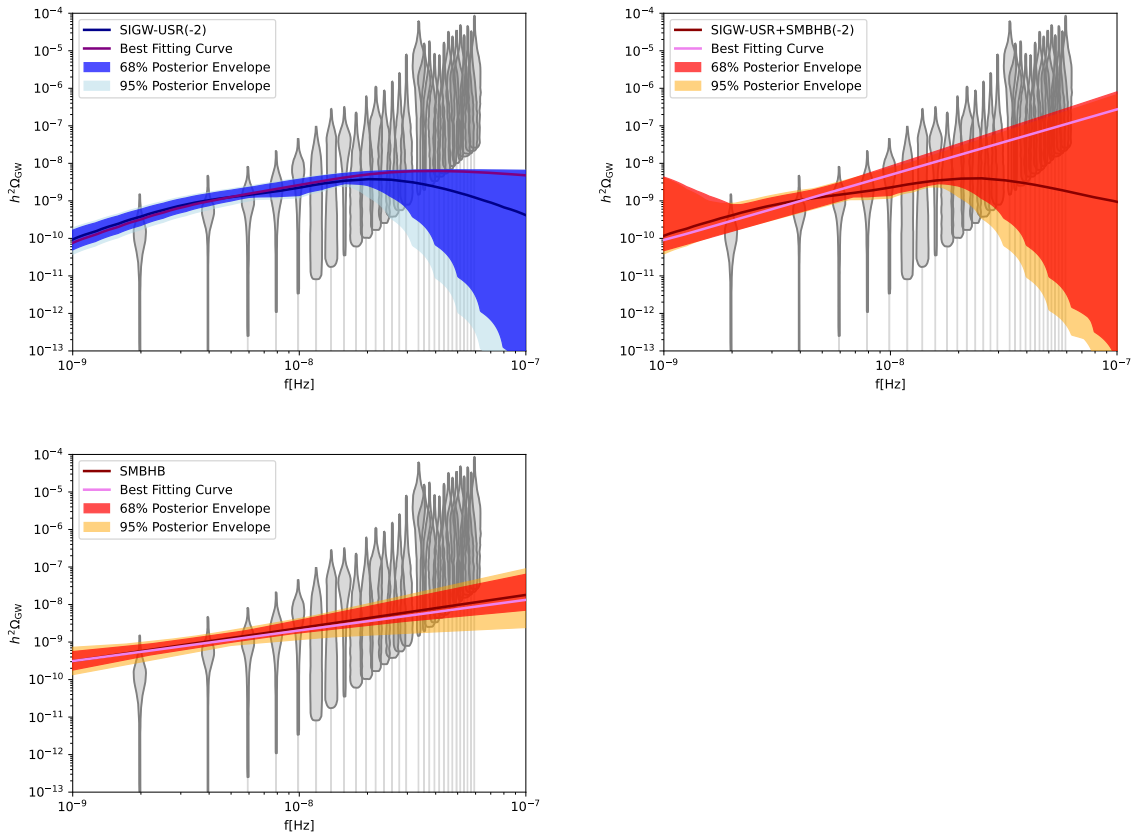


Figure 5. The 68% and 95% posterior envelopes, the best-fitting SGWB power spectra, and the median SGWB power spectra for the SIGW-USR, SIGW-USR+SMBHB, and SMBHB models, all using astrophysical priors, are shown. The median GW power spectra labels are used to indicate which model each figure corresponds to. Since these figures don't show the P_{Rp} parameter directly, we mark (-2) to remind readers of the upper limit $\log_{10} P_{\text{Rp}} \leq -2$.

5 Conclusions and discussions

In this work, we explore the possibility of using USR inflation to explain the NG15 dataset and obtain the favored physical parameter space of the USR regime by the data. The posterior distributions indicate strong degeneracy between $\log_{10} P_{\text{Rp}}$ and $\log_{10} f_p$, and between N and ΔN . We obtain the 95% C.L. lower limit $\Delta N > 2.8$ for $N \approx 20$, regardless of the value of β . In our previous work [89], the upper limit of ΔN given by the LIGO-Virgo O3 dataset is about 2.87 for $N \approx 41.5$ with $\beta = 1$. Compared to the LIGO-Virgo data, the NG15 dataset places strong constraints on ΔN .

In Fig. 2, we find that the best fitting spectra and the posterior envelopes from SIGW-USR alone and SIGW-USR+SMBHB are similar to each other. To compare the goodness of fit to the data for different models, one can calculate the Bayes factor. Our results reveal that the Bayes factors for the SIGW-USR model and the combined SIGW-USR+SMBHB model are comparable to the best-fit model reported in Ref. [5]. Incorporating SMBHB leads to an increase in the Bayes factor. This enhancement can be attributed to the ability of the SMBHB spectrum to compensate for the insufficient fit of the SIGW-USR model alone,

thereby enhancing the likelihood.

For the power spectrum of curvature perturbations, we place the limit $\log_{10} P_{\text{Rp}} > -1.95$ at 95% C.L.. Moreover, the one-dimensional posteriors of $\log_{10} P_{\text{Rp}}$ and $\log_{10} f_{\text{p}}$ show the presence of peaks in the NANOGrav sensitivity band. The peaks can also be found in the SIGW-Gauss model in [5] when Δ is small, where Δ is the scale parameter of the Gauss distribution characterizing the shape of P_{R} .

In Ref. [5], three SIGW models are investigated, mathematically modeled by different power spectrum $P_{\text{R}}(k)$. The contours of $\log_{10} A - \log_{10} f_{\star}$ in [5] are quite similar with $\log_{10} P_{\text{Rp}} - \log_{10} f_{\text{p}}$ in this work. The reason for this is that the parameters in our model are similar to that of the SIGW models in [5], such as the infrared index, the peak amplitude, and the peak frequency. However, note that the energy spectrum in this work is directly calculated from USR inflation.

To avoid the overproduction of PBHs, we apply the conservative upper bound, $\log_{10} P_{\text{Rp}} \leq -2$, for Gaussian curvature perturbations.² In this case, the SMBHB and SIGW-USR models fit the NG15 dataset almost equally well. In Fig. 5, due to the 2-D Gaussian prior, the power-law cannot exhibit a steeper slope or larger amplitude, leading to poor performance in the lower frequency bins. For the SIGW-USR model, the upper limit on P_{Rp} forces the peak to occur early, resulting in a poor fit for the frequency bins to the right of 10^{-8} Hz. Although the combination of the best SGWB power spectra from these two models does not provide a significantly better fit to the NG15 dataset, this combination helps improve the poor performance of certain curves. However, as pointed out by many papers [21, 23, 31, 33, 93, 94], the primordial non-Gaussianities, even with a small value $f_{\text{nl}} \lesssim -0.5$, can largely alleviate this problem and reduce the PBH abundance results from large curvature perturbations. Primordial non-Gaussianities have been widely investigated as the method to detect the interactions of inflaton and distinguish other mechanisms that generating primordial curvature perturbations from CMB and large-scale structure observations [95–97]. The matter collapse into PBHs in the Hubble horizons where curvature perturbations exceed the threshold \mathcal{R}_c . Since \mathcal{R}_c is generally more than 5 times the standard deviation of curvature perturbations, a small correction on \mathcal{R}_c can significantly enhance or depress the initial PBH abundance. The presence of non-Gaussianity can shift the threshold of PBH formation. The threshold can be lifted to suppress the PBH abundance with the help of a negative f_{nl} , allowing a released upper bound on P_{Rp} . Even a small value of $|f_{\text{nl}}|$, is enough to make the USR model much more preferred by data. The Bayes factor with the upper bound $P_{\text{Rp}} < 10^{-1.5}$ is already close to the case without upper any bounds on P_{Rp} . Therefore, we also obtain the result with $\log_{10} P_{\text{Rp}} \leq -1.5$, which indicates that the upper bound $\log_{10} P_{\text{Rp}} \leq -1.5$ captures most of the best-fit regions. In this case, the USR model is significantly preferred by data compared to the SMBHB model.

We also provide the analysis of SIGWs from another type of $P_{\text{R}}(k)$ which is induced by various GW sources after inflation [98–101] and has a characteristic k^3 slope at the infrared side because of causality. At the ultraviolet side, we set a cutoff at the scale where the central-limit theorem becomes invalid. The posterior distribution is shown in Fig. 6, which is quite similar to Fig. 1, since the precision of current data is not high enough to distinguish the slope k^3 and k^4 . The result with a slope of k^3 agrees well with the previous one with a

² Ω_{GW} is also constrained by the observations of the effective freedom of relativistic particles from CMB experiments. The constraint turns out to be roughly $\Omega_{\text{GW}} \lesssim 3 \times 10^{-7}$ for the future CMB-S4 mission [90–92], which already exceeds the GW strength observed by PTA experiments for about one order of magnitude. Therefore, considering the constraint from Δ_{eff} has negligible impact on the results.

large β since this cutoff model can be treated as an extreme USR model.

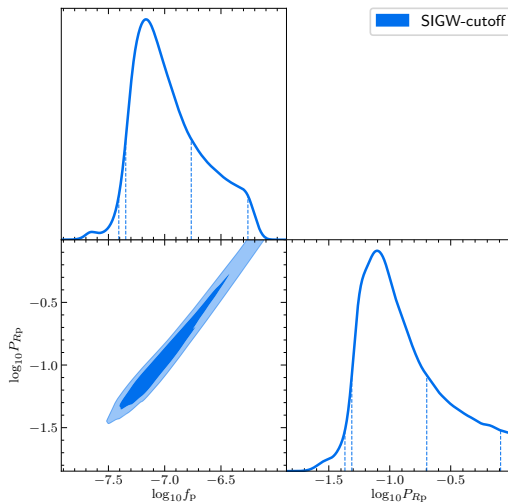


Figure 6. Posterior distribution of the parameters in the cutoff induced SIGW. The red and blue lines denote the 68% and 95% confidence regions, respectively.

Acknowledgments

We sincerely thank Zu-Cheng Chen for the helpful discussion. This work is supported in part by the National Key Research and Development Program of China Grant No. 2020YFC2201501 and No. 2020YFC2201502, in part by the National Natural Science Foundation of China under Grant No. 12075297, No. 12235019 and No. 12105060.

A The choice of γ value

In the parameterization of the power spectrum of curvature perturbations in USR inflation, the parameter γ characterizes the smoothness of $P_R(k)$ around the peak. We compare our parameterization curves with the predictions of $P_R(k)$ from numerical simulations of many USR models and find that $\gamma = 2.6$ is a representative parameter value.

Besides, we explore the influence of varying γ values on the results. We employ $\gamma = 1$ and $\gamma = 5$ to fit the NG15 dataset, and the results are illustrated in Fig. 7. Comparing with Fig. 1, we find that the selection of γ has a negligible effect on the constraints. Only minor differences can be observed in the region of $\beta < 1$. With α fixed, large γ and small β lead to significant smoothing, causing a substantial increase in $P_R(k)$. As a consequence, the peak frequency is expected to shift towards higher frequencies to match the observed data.

Based on the above considerations, we fix $\gamma = 2.6$ in this paper.

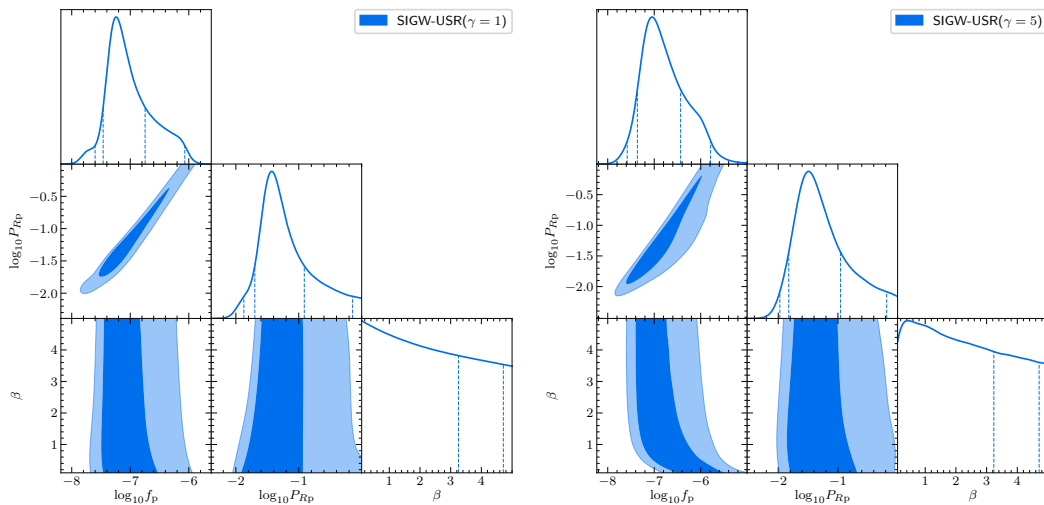


Figure 7. Posterior distribution of the parameters in the USR-SIGW model where γ is chosen as 1 (left panel) and 5 (right panel). The red and blue lines denote the 68% and 95% confidence regions, respectively.

References

- [1] B. P. Abbott et al., *Physical Review Letters* **116**, 061102 (2016).
- [2] R.-G. Cai, Z. Cao, Z.-K. Guo, S.-J. Wang, and T. Yang, *Natl. Sci. Rev.* **4**, 687 (2017), [1703.00187](#).
- [3] L. Bian et al., *Sci. China Phys. Mech. Astron.* **64**, 120401 (2021), [2106.10235](#).
- [4] H. Xu et al., *Res. Astron. Astrophys.* **23**, 075024 (2023), [2306.16216](#).
- [5] A. Afzal et al. (NANOGrav), *Astrophys. J. Lett.* **951** (2023), [2306.16219](#).
- [6] D. J. Reardon et al., *Astrophys. J. Lett.* **951** (2023), [2306.16215](#).
- [7] J. Antoniadis et al. (2023), [2306.16214](#).
- [8] G. Agazie et al. (2023), [arXiv:2306.16213](#).
- [9] G. Agazie et al. (NANOGrav), *Astrophys. J. Lett.* **952**, L37 (2023), [2306.16220](#).
- [10] C. Han, K.-P. Xie, J. M. Yang, and M. Zhang, *Phys. Rev. D* **109**, 115025 (2024), [2306.16966](#).
- [11] S. Jiang, A. Yang, J. Ma, and F. P. Huang (2023), [2306.17827](#).
- [12] K. Fujikura, S. Girmohanta, Y. Nakai, and M. Suzuki, *Phys. Lett. B* **846**, 138203 (2023), [2306.17086](#).
- [13] J. Ellis, M. Lewicki, C. Lin, and V. Vaskonen (2023), [2306.17147](#).
- [14] Z. Wang, L. Lei, H. Jiao, L. Feng, and Y.-Z. Fan (2023), [2306.17150](#).
- [15] G. Lazarides, R. Maji, and Q. Shafi (2023), [2306.17788](#).
- [16] N. Kitajima, J. Lee, K. Murai, F. Takahashi, and W. Yin (2023), [2306.17146](#).
- [17] Y. Gouttenoire and E. Vitagliano (2023), [2306.17841](#).
- [18] Z.-C. Chen, C. Yuan, and Q.-G. Huang, *Phys. Rev. Lett.* **124**, 251101 (2020), [1910.12239](#).
- [19] E. Madge, E. Morgante, C. Puchades-Ibáñez, N. Ramberg, W. Ratzinger, S. Schenk, and P. Schwaller, *JHEP* **23**, 171 (2020), [2306.14856](#).
- [20] K. Inomata, K. Kohri, and T. Terada (2023), [2306.17834](#).
- [21] L. Liu, Z.-C. Chen, and Q.-G. Huang (2023), [2307.01102](#).
- [22] Z.-Q. You, Z. Yi, and Y. Wu (2023), [2307.04419](#).
- [23] S. Wang, Z.-C. Zhao, J.-P. Li, and Q.-H. Zhu (2023), [2307.00572](#).
- [24] Z.-C. Zhao, Q.-H. Zhu, S. Wang, and X. Zhang (2023), [2307.13574](#).
- [25] S. Basilakos, D. V. Nanopoulos, T. Papanikolaou, E. N. Saridakis, and C. Tzerefos (2023), [2307.08601](#).
- [26] S. Basilakos, D. V. Nanopoulos, T. Papanikolaou, E. N. Saridakis, and C. Tzerefos (2023), [2309.15820](#).
- [27] J.-H. Jin, Z.-C. Chen, Z. Yi, Z.-Q. You, L. Liu, and Y. Wu, *JCAP* **09**, 016 (2023), [2307.08687](#).
- [28] L. Liu, Z.-C. Chen, and Q.-G. Huang (2023), [2307.14911](#).
- [29] L. Liu, Y. Wu, and Z.-C. Chen (2023), [2310.16500](#).
- [30] H. Firouzjahi and A. Talebian, *JCAP* **10**, 032 (2023), [2307.03164](#).
- [31] G. Franciolini, A. Iovino, Junior., V. Vaskonen, and H. Veermae (2023), [2306.17149](#).
- [32] J. Ellis, M. Fairbairn, G. Franciolini, G. Hütsi, A. Iovino, M. Lewicki, M. Raidal, J. Urrutia, V. Vaskonen, and H. Veermäe (2023), [2308.08546](#).

- [33] S. Choudhury, K. Dey, A. Karde, S. Panda, and M. Sami (2023), [2310.11034](#).
- [34] S. Choudhury, A. Karde, S. Panda, and M. Sami (2023), [2308.09273](#).
- [35] J. Liu, Z.-K. Guo, and R.-G. Cai, Phys. Rev. D **101**, 083535 (2020), [2003.02075](#).
- [36] O. Özsoy and G. Tasinato, JCAP **04**, 048 (2020), [1912.01061](#).
- [37] C. T. Byrnes, P. S. Cole, and S. P. Patil, JCAP **06**, 028 (2019), [1811.11158](#).
- [38] S. Pi and J. Wang (2022), [2209.14183](#).
- [39] J. Lin, Q. Gao, Y. Gong, Y. Lu, C. Zhang, and F. Zhang, Phys. Rev. D **101**, 103515 (2020), [2001.05909](#).
- [40] Z. Yi (2022), [2206.01039](#).
- [41] S. Kawai and J. Kim, Phys. Rev. D **104**, 083545 (2021), [2108.01340](#).
- [42] S. Kawai and J. Kim, Phys. Rev. D **104**, 043525 (2021), [2105.04386](#).
- [43] M. Cicoli, V. A. Diaz, and F. G. Pedro, JCAP **06**, 034 (2018), [1803.02837](#).
- [44] M. Cicoli, F. G. Pedro, and N. Pedron, JCAP **08**, 030 (2022), [2203.00021](#).
- [45] O. Özsoy, S. Parameswaran, G. Tasinato, and I. Zavala, JCAP **07**, 005 (2018), [1803.07626](#).
- [46] I. Dalianis, A. Kehagias, and G. Tringas, JCAP **01**, 037 (2019), [1805.09483](#).
- [47] T.-J. Gao and Z.-K. Guo, Phys. Rev. D **98**, 063526 (2018), [1806.09320](#).
- [48] L. Wu, Y. Gong, and T. Li, Phys. Rev. D **104**, 123544 (2021), [2105.07694](#).
- [49] S. Kawai and J. Kim, Phys. Rev. D **107**, 043523 (2023), [2209.15343](#).
- [50] S. S. Mishra and V. Sahni, JCAP **04**, 007 (2020), [1911.00057](#).
- [51] O. Özsoy and Z. Lalak, JCAP **01**, 040 (2021), [2008.07549](#).
- [52] B.-M. Gu, F.-W. Shu, K. Yang, and Y.-P. Zhang (2022), [2207.09968](#).
- [53] S. Choudhury and A. Mazumdar, Phys. Lett. B **733**, 270 (2014), [1307.5119](#).
- [54] C. Germani and T. Prokopec, Phys. Dark Univ. **18**, 6 (2017), [1706.04226](#).
- [55] N. Bhaumik and R. K. Jain, JCAP **01**, 037 (2020), [1907.04125](#).
- [56] K. Kefala, G. P. Kodaxis, I. D. Stamou, and N. Tetradis, Phys. Rev. D **104**, 023506 (2021), [2010.12483](#).
- [57] K. Inomata, E. McDonough, and W. Hu, Phys. Rev. D **104**, 123553 (2021), [2104.03972](#).
- [58] Y.-F. Cai, X.-H. Ma, M. Sasaki, D.-G. Wang, and Z. Zhou, Phys. Lett. B **834**, 137461 (2022), [2112.13836](#).
- [59] K. Inomata, E. McDonough, and W. Hu, JCAP **02**, 031 (2022), [2110.14641](#).
- [60] B. Carr, F. Kuhnel, and M. Sandstad, Phys. Rev. D **94**, 083504 (2016), [1607.06077](#).
- [61] S. Bird, I. Cholis, J. B. Muñoz, Y. Ali-Haïmoud, M. Kamionkowski, E. D. Kovetz, A. Raccanelli, and A. G. Riess, Phys. Rev. Lett. **116**, 201301 (2016), [1603.00464](#).
- [62] H. Di and Y. Gong, JCAP **07**, 007 (2018), [1707.09578](#).
- [63] J. Garcia-Bellido and E. Ruiz Morales, Phys. Dark Univ. **18**, 47 (2017), [1702.03901](#).
- [64] M. P. Hertzberg and M. Yamada, Phys. Rev. D **97**, 083509 (2018), [1712.09750](#).
- [65] S. Passaglia, W. Hu, and H. Motohashi, Phys. Rev. D **99**, 043536 (2019), [1812.08243](#).
- [66] R.-g. Cai, S. Pi, and M. Sasaki, Phys. Rev. Lett. **122**, 201101 (2019), [1810.11000](#).
- [67] C. Fu, P. Wu, and H. Yu, Phys. Rev. D **102**, 043527 (2020), [2006.03768](#).

- [68] Y.-F. Cai, X.-H. Ma, M. Sasaki, D.-G. Wang, and Z. Zhou (2022), [2207.11910](#).
- [69] D. G. Figueroa, S. Raatikainen, S. Rasanen, and E. Tomberg, JCAP **05**, 027 (2022), [2111.07437](#).
- [70] D. G. Figueroa, S. Raatikainen, S. Rasanen, and E. Tomberg, Phys. Rev. Lett. **127**, 101302 (2021), [2012.06551](#).
- [71] S. Pi and M. Sasaki (2021), [2112.12680](#).
- [72] Q. Wang, Y.-C. Liu, B.-Y. Su, and N. Li, Phys. Rev. D **104**, 083546 (2021), [2111.10028](#).
- [73] W.-T. Xu, J. Liu, T.-J. Gao, and Z.-K. Guo, Phys. Rev. D **101**, 023505 (2020), [1907.05213](#).
- [74] D. Y. Cheong, S. M. Lee, and S. C. Park, JCAP **01**, 032 (2021), [1912.12032](#).
- [75] M. Braglia, D. K. Hazra, F. Finelli, G. F. Smoot, L. Sriramkumar, and A. A. Starobinsky, JCAP **08**, 001 (2020), [2005.02895](#).
- [76] N. Aghanim et al. (Planck), Astron. Astrophys. **641**, A6 (2020), [Erratum: Astron.Astrophys. 652, C4 (2021)], [1807.06209](#).
- [77] R. Emami and G. Smoot, JCAP **01**, 007 (2018), [1705.09924](#).
- [78] A. D. Gow, C. T. Byrnes, P. S. Cole, and S. Young, JCAP **02**, 002 (2021), [2008.03289](#).
- [79] B. Cyr, T. Kite, J. Chluba, J. C. Hill, D. Jeong, S. K. Acharya, B. Bolliet, and S. P. Patil (2023), [2309.02366](#).
- [80] C. Pattison, V. Vennin, H. Assadullahi, and D. Wands, JCAP **08**, 048 (2018), [1806.09553](#).
- [81] W. G. Lamb, S. R. Taylor, and R. van Haasteren, *The need for speed: Rapid refitting techniques for bayesian spectral characterization of the gravitational wave background using ptas* (2023), [2303.15442](#).
- [82] J. A. Ellis, M. Vallisneri, S. R. Taylor, and P. T. Baker, *Enterprise: Enhanced numerical toolbox enabling a robust pulsar inference suite*, Zenodo (2020), URL <https://doi.org/10.5281/zenodo.4059815>.
- [83] M. Vallisneri, S. R. Taylor, J. Simon, et al., The Astrophysical Journal **893**, 112 (2020), URL <https://doi.org/10.3847/2F1538-4357/2Fab7b67>.
- [84] R. W. Hellings and G. S. Downs, ApJ **265**, L39 (1983).
- [85] K. Kohri and T. Terada, Phys. Rev. D **97**, 123532 (2018), [1804.08577](#).
- [86] J. R. Espinosa, D. Racco, and A. Riotto, JCAP **09**, 012 (2018), [1804.07732](#).
- [87] K. Saikawa and S. Shirai, Journal of Cosmology and Astroparticle Physics **2020**, 011 (2020), URL <https://dx.doi.org/10.1088/1475-7516/2020/08/011>.
- [88] J. Silk and M. S. Turner, Phys. Rev. D **35**, 419 (1987).
- [89] B. Mu, G. Cheng, J. Liu, and Z.-K. Guo, Physical Review D **107** (2023), URL <https://doi.org/10.1103/2Fphysrevd.107.043528>.
- [90] K. N. Abazajian et al. (CMB-S4) (2016), [1610.02743](#).
- [91] D. Baumann, D. Green, J. Meyers, and B. Wallisch, JCAP **01**, 007 (2016), [1508.06342](#).
- [92] J. Cang, Y.-Z. Ma, and Y. Gao, Astrophys. J. **949**, 64 (2023), [2210.03476](#).
- [93] C. Yuan, D.-S. Meng, and Q.-G. Huang, JCAP **12**, 036 (2023), [2308.07155](#).
- [94] S. Pi (2024), [2404.06151](#).
- [95] N. Bartolo, E. Komatsu, S. Matarrese, and A. Riotto, Phys. Rept. **402**, 103 (2004), [astro-ph/0406398](#).
- [96] X. Chen, Adv. Astron. **2010**, 638979 (2010), [1002.1416](#).

- [97] Y. Akrami et al. (Planck), *Astron. Astrophys.* **641**, A9 (2020), [1905.05697](#).
- [98] J. Liu, L. Bian, R.-G. Cai, Z.-K. Guo, and S.-J. Wang, *Phys. Rev. Lett.* **130**, 051001 (2023), [2208.14086](#).
- [99] Z.-M. Zeng, J. Liu, and Z.-K. Guo, *Phys. Rev. D* **108**, 063005 (2023), [2301.07230](#).
- [100] T. Papanikolaou, V. Vennin, and D. Langlois, *JCAP* **03**, 053 (2021), [2010.11573](#).
- [101] G. Domènech, C. Lin, and M. Sasaki, *JCAP* **04**, 062 (2021), [Erratum: *JCAP* 11, E01 (2021)], [2012.08151](#).